Research article

Effect of chloride ion concentration, spraying time and pH values on corrosion behavior of friction stir welded AZ61A magnesium alloy welds in salt fog environments

A. Dhanapal[a]*, S. Rajendra Boopathy[b], V. Balasubramanian[c]

[a]Department of Mechanical Engineering, Sri Ramanujar Engineering College, Vandalur, Chennai, Tamil Nadu, India
[b]Department of Mechanical Engineering,College of Engineering, Guindy, Anna University, Chennai, Tamil Nadu, India
[c]Center for Materials Joining & Research (CEMAJOR), Department of Manufacturing Engineering, Annamalai University, Annamalainagar, Chidambaram, Tamil Nadu, India

Abstract

The present research devoted to the investigation of the corrosion behavior of AZ61A FSW welds in accelerated conditions, including the influence of salt fog environmental parameters such as chloride ion concentration, pH, and duration of exposure. Significant numbers of tests were carried out that make possible to create the regression model (empirical equation) of influence of selected environmental parameters on corrosion rate. The corrosion products were analyzed by SEM and XRD analysis. This research demonstrates the effect of chloride ion concentrations, spraying time and pH values on corrosion rate, and it show the corrosion activity decelerates with the increasing pH value and spraying time respectively. It was found that the increase in chloride ion concentration accelerates the corrosion of AZ61A weldments. The corrosion morphology was predominantly influenced by the distribution of β-phase (e.g. $Mg_{17}Al_{12}$ intermetallic).

©2013 Usak University all rights reserved.

Keywords: Magnesium alloy, friction stir welding, salt fog tests, weight loss, corrosion rate

1. Introduction

The magnesium alloys are promising candidate to replace steel and aluminum in many structural and mechanical applications due to their attractive properties. They have an outstanding strength-to-weight ratio, good castability, high damping capacity as well as recyclability [1]. The joining of magnesium components made from this alloy is, however, still limited. Unfortunately, conventional fusion welding of magnesium alloys often produces porosity and hot cracking in the welded joint. This deteriorates both the mechanical properties as well as corrosion resistance [2, 3]. Hence, it will be of extreme benefit if a solid-state joining process, i.e. one which avoids bulk melting of the base material, can be developed and implemented for joining of magnesium alloys.

However, a recent innovation of Friction Stir Welding (FSW) process eliminated the above said problems. FSW is a solid state, autogenous process; and hence there is no melting and solidification. Though the mechanical properties and micro structural characteristics of FSW joints of Mg alloys are the topic of many researchers, the corrosion properties of these joints have not yet been fully explored. The overall corrosion processes can be described by three stages. The first stage corresponds to the pit nucleation and growth; the second stage involves the growth of a passive oxide layer; and the third stage involves the reactivation [4].

The influence of pH and/or chloride ion concentration on the corrosion of pure magnesium and magnesium alloys has been studied extensively for understanding of environmental factors controlling corrosion [5]. The pH of tests solution has a considerable effect on the corrosion rate of Mg. However, it is difficult to keep it consistent, especially in a neutral solution, because the corrosion product of Mg, Mg hydroxide is readily dissolved into the solution which results in substantial pH increase [6]. Corrosion attack of Mg, AZ31, AZ80 and AZ91D materials under the salt fog tests increased with increasing temperature and chloride ion concentration [7]. Individual pitting characteristics, including pit surface area and pit volume, were greater for the salt spray surfaces [8]. Usually, the second phase in traditional Mg alloys consists of binary alloy such as $Mg_{17}Al_{12}$ & AlMn. Both pitting and filiform corrosion can access to the Mg alloy containing binary phase [9-12]. The general and pitting corrosion behavior of parent and FSW nugget regions were nearly the same even though they were different in the untreated condition. The corrosion morphology of the AM50 alloy was predominantly controlled by the β phase distribution. Pitting corrosion was discerned in the welds [13, 14].

From the literature review, it is understood that most of the research information on corrosion behavior of Mg alloys focused on pitting corrosion and general corrosion of unwelded base alloys. Hence, the present investigation was carried out to study the effect of chloride ion concentrations, spraying time and pH values on corrosion behavior of AZ61A mg alloy weldments and incorporating the varying parameters under salt fog environments.

2. Experimental Work

2.1. Sample Preparation

The material used in this study was AZ61A magnesium alloy in the form of extruded plates of 6 mm thickness. The chemical composition and mechanical properties of the base metal are presented in Table 1 and Table 2. The optical micrograph of base metal and stir zone of FSW joint of AZ61A Mg alloy is shown in Fig. 1. The plate was cut to a required size (300mm x 150mm) by power hacksaw followed by milling. The square butt joint configuration was prepared to fabricate the joints. The initial joint configuration was obtained by securing the plates in position using mechanical clamps. The direction of welding was normal to the extruded direction. Single pass welding procedure was followed to fabricate the joints. A non-consumable tool made of high carbon steel was used to fabricate joints. An indigenously designed and developed computer numerical controlled FSW machine (22kW, 4000RPM, 60kN) was used to fabricate joints. The FSW parameters were optimized by conducting trial runs, and the welding conditions which produced defect free joints were taken as optimized welding conditions. The optimized welding conditions used to fabricate the joints in this investigation are presented in Table 3. The welded joints were sliced using a power hacksaw, and then machined to the

required dimensions to prepare for the corrosion tests. Friction stir welds were sliced and the different regions of cut section of FSW joints as shown in Fig. 2. From the welded joints, the corrosion tests specimens were extracted from the friction stir welds to the dimensions of 50 mm x 16 mm x 6 mm shown in Fig. 3. The optical micrograph of base metal and stir zone of FSW joint of AZ61A Mg alloy is shown in Fig. 4. The specimens were ground with 500#, 800#, 1200#, 1500# grit SiC paper. Finally, it was cleaned with acetone and washed in distilled water then dried by warm flowing air.

Table 1
Chemical composition (wt%) of AZ61A Mg alloy

Al	Zn	Mn	Mg
5.45	1.26	0.17	Balance

Table 2
Mechanical Properties of AZ61A Mg alloy

Yield Strength (MPa)	Ultimate Tensile Strength (MPa)	Elongation (%)	Vickers hardness at 0.05 kg load (Hv)
177	272	8.40	57

Table 3
Optimized welding conditions and process parameters used to fabricate the joints

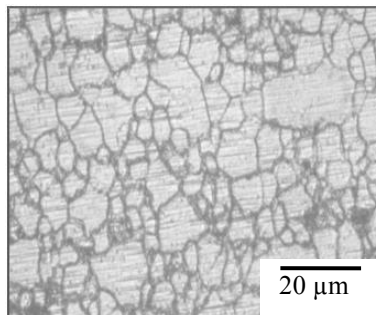| Rotational speed (rpm)	Welding speed (mm/min)	Axial force (kN)	Tool shoulder diameter (mm)	Pin diameter (mm)	Pin length (mm)	Pin profile
1000	75	3	18	6	5	Left hand thread of 1mm pitch

Fig. 1 Optical micrograph of AZ61A base metal

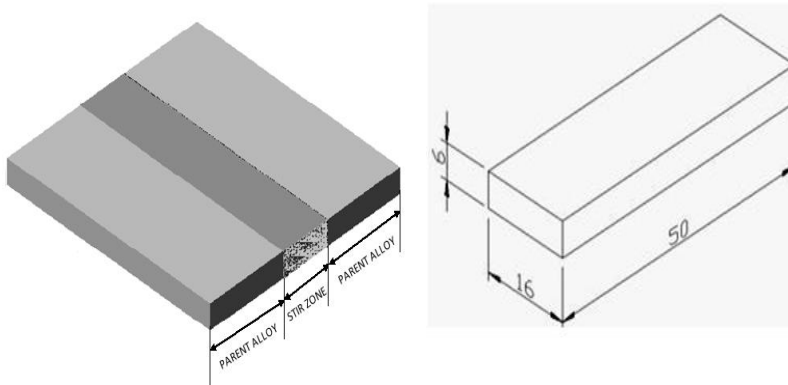**Fig. 2** Macrostructure of Different Regions of FSW joints

149

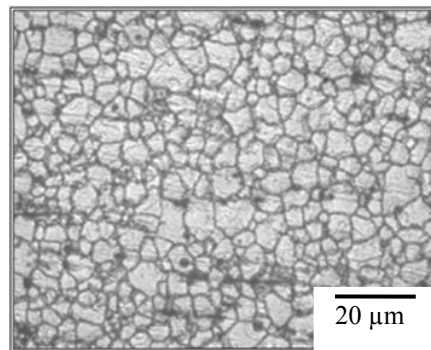**Fig. 3** Dimensions of corrosion tests specimen

20 µm

Fig. 4 Optical micrograph of stir zone of FSW AZ61A Mg alloy

2.2. Corrosion Test Parameters

From the literature [15-18], the predominant factors that have a greater influence on corrosion behavior of AZ61A magnesium alloy are identified. They are: (i) chloride ion concentration, (ii) spraying time, (iii) pH values of the solution. Large numbers of trial experiments were conducted to identify the feasible testing conditions using friction stir welded AZ61A magnesium alloy weld metal region under spraying conditions. The following inferences are obtained:

1. If pH value of the solution was less than 3, then the change in chloride ion concentration did not considerably affect the corrosion.
2. If the pH value was between 3 to 11, an inhibition of the corrosion process had occurred stabilizing the protective layer.
3. If pH value was greater than 11, blocking of further corrosion by the active centers of protective layer took place.
4. If the chloride ion concentration was less than 0.2M, visible corrosion did not occur in the experimental period.
5. If the chloride ion concentration was in between the 0.2M to 1M, there was a reasonable fluctuation in the corrosion rate.
6. If the chloride ion concentration was greater than 1M, rise in corrosion rate was slightly decreased.

7. If the spraying time was less than 1 hr, the surface was completely covered with the thick and rough corrosion products and had an unpredicted corrosion rate.
8. If the spraying time was in between 1 to 9 hrs, the tracks of the corrosion could be predicted.
9. If the spraying time was greater than 9 hrs, the tracks of corrosion film were difficult to identify.

2.3. Developing the experimental design matrix

Owing to a wide range of factors, the use of three factors and central composite rotatable design matrix was chosen to minimize number of experiments. The assay conditions for the reaction parameters were taken at zero level (center point) and one level (+1 and 1). The design was extended up to a ±α (axial point) of 1.68. The center values for variables were carried out at least six times for the estimation of error and single runs for each of the other combinations; twenty runs were done in a totally random order. The design would consist of the eight corner points, the six star points, and m center points. The star points have $\alpha = 8^{0.25} = 1.682$. Design matrix consisting 20 sets of coded conditions (composing a full replication three factorial of 8 points, six corner points and six centre points) was chosen in this investigation. Table 4 presents the ranges of factors considered, and Table 5 shows the 20 sets of coded and actual values used to conduct the experiments. The coded values of any intermediate values could be calculated using following relationship:

$$X_i = 1.682 \ [2X – (X_{max} - X_{min})] \ / \ (X_{max} - X_{min}) \tag{1}$$

where, X_i is the required coded values of a variable X and X is any values of the variable from X_{min} to X_{max}; X_{min} is the lower level of the variable; X_{max} is the upper level of the variable.

2.4. Recording the Responses

Solution of NaCl with concentrations of 0.2M, 0.36M, 0.6M, 0.84M, and 1M were prepared. The pH values of the solution were maintained as pH 3, pH 4.62, pH 7, pH 9.38, and pH 11 with concentrated HCl and NaOH respectively. The pH values were measured using a digital pH meter. The tests method consists of exposing the specimens in a salt spray chamber as per ASTM B 117 standards and evaluating the corrosion tested specimen with the method as per ASTM G1-03[16,17]. Basically, the salt spray tests procedure involves the spraying of a salt solution onto the samples being tested. This was done inside a temperature controlled chamber. The glass racks were contained in the salt fog chamber. The samples under tests were inserted into the chamber, following which the salt-containing solution was sprayed as a very fine fog mist over the samples. NaCl in tapped water was pumped from a reservoir to spray nozzles. The solution was mixed with humidified compressed air at the nozzle and this compressed air atomized the NaCl solution into a fog at the nozzle. Heaters were maintained at 35°C cabinet temperature. Within the chamber, the samples were rotated frequently so that all samples were exposed uniformly to the salt spray mist. The temperature within the chamber was maintained at a constant level. Since the spray was continuous, the samples were continuously wet, and therefore, uniformly subjected to corrosion. The corrosion rate of the friction stir welded AZ61A alloy specimen was estimated by weight loss measurement. The original weight (w_o) of the specimen was recorded, and then the specimen was sprayed with the solution of NaCl for different spraying times of 1, 2.62, 5, 7.38 and 9 hrs.

Table 4
Important factors and their levels

SI. No	Factor	Unit	Notation	Levels				
				-1.682	-1	0	+1	+1.682
1	pH values		P	3	4.62	7	9.38	11
2	Immersion time	hr	T	1	2.62	5	7.38	9
3	Cl⁻ Concentration	M	C	0.2	0.36	0.6	0.84	1

Table 5
Design matrix and Experimental results

Ex. No	Coded valuess			Actual valuess			Weight loss (g)	Corrosion rate (mm/year)
	pH (P)	Time (T)	Conc. (C)	pH (P)	Time (hr)	Conc. (M)		
1	-1	-1	-1	4.62	2.62	0.36	0.0087	14.62 (0.11)
2	+1	-1	-1	9.38	2.62	0.36	0.0061	10.23 (0.56)
3	-1	+1	-1	4.62	7.38	0.36	0.0144	11.89 (0.21)
4	+1	+1	-1	9.38	7.38	0.36	0.0126	8.99 (0.18)
5	-1	-1	+1	4.62	2.62	0.84	0.0130	15.82 (0.16)
6	+1	-1	+1	9.38	2.62	0.84	0.0075	11.31 (0.10)
7	-1	+1	+1	4.62	7.38	0.84	0.0145	12.92 (0.26)
8	+1	+1	+1	9.38	7.38	0.84	0.0209	10.75 (0.05)
9	-1.682	0	0	3	5	0.60	0.0267	17.96 (0.26)
10	+1.682	0	0	11	5	0.60	0.0102	10.88 (0.41)
11	0	-1.682	0	7	1	0.60	0.0047	11.23 (0.56)
12	0	+1.682	0	7	9	0.60	0.0165	8.51 (0.42)
13	0	0	-1.682	7	5	0.20	0.0200	11.66 (0.23)
14	0	0	+1.682	7	5	1	0.0200	15.28 (0.40)
15	0	0	0	7	5	0.60	0.0120	9.89 (0.36)
16	0	0	0	7	5	0.60	0.0120	9.89 (0.36)
17	0	0	0	7	5	0.60	0.0120	9.89 (0.36)
18	0	0	0	7	5	0.60	0.0120	9.89 (0.36)
19	0	0	0	7	5	0.60	0.0120	9.89 (0.36)
20	0	0	0	7	5	0.60	0.0120	9.89 (0.36)

The values presented in bracket are the standard deviation.

The corrosion products were removed by immersing the specimens for one minute in a solution prepared by using 50 g chromium trioxide (CrO_3), 2.5 g silver nitrate ($AgNO_3$) and 5 g barium nitrate($Ba(NO_3)_2$) for 250 ml distilled water. The corrosion rate of FSW joints of AZ61A was calculated by using the following equation as per the ASTM standards B117,

$$\text{Corrosion rate (mm/year)} = \frac{8.76 \times 10^4 \times w}{A \times D \times T} \tag{2}$$

where; w is weight loss in grams, A is surface area of the specimen in cm², D is the density of the material as 1.72 g/cm³, and T is spraying time in hours.

Microstructural analysis on the corroded specimens was carried out using a light optical microscope (Make: Union Optics, Japan; Model: VERSAMET-3) incorporated with an image analyzing software (Clemex-vision). The exposed specimen surface was prepared for the micro examination in the "as polished" conditions. The corrosion tests specimens were polished in disc polishing, machine with minor polishing and the surface was observed at 200X magnification. The corrosion products were analyzed by SEM EDAX and XRD analysis.

3. Developing an Empirical Relationship

In the present investigation, to correlate the salt spray tests parameters and the corrosion rate of welds, a second order quadratic model was developed. The response (corrosion rate) is a function of pH values (P), spraying time (T) and chloride ion concentration (C), and it could be expressed as:

$$\text{Corrosion rate (CR)} = f\,(P, T, C) \qquad (3)$$

The empirical relationship must include the main and interaction effects of all factors; and hence the selected polynomial is expressed as follows:

$$Y = b_o + \Sigma b_i\, x_i + \Sigma\, b_{ii}\, x_j + \Sigma\, b_{ij}\, x_i\, x_j \qquad (4)$$

For three factors, the selected polynomial could be expressed as

$$\text{Corrosion Rate CR} = b_0 + b_1\,(P) + b_2\,(T) + b_3\,(C) + b_{11}\,(P^2) + b_{22}\,(T^2)$$
$$+\, b_{33}\,(C^2) + b_{12}\,(PT) + b_{13}\,(PC) + b_{23}\,(TC) \qquad (5)$$

Where b_0 is the average of responses (corrosion rate) and b_1, b_2, b_3, b_{11}, b_{12}, b_{13}, b_{22}, b_{23}, b_{33} are the coefficients that depend on their respective main and interaction factors, which were calculated using the expression given below:

$$B_i = \Sigma\,(X_i, Y_i)\,/\,n \qquad (6)$$

Where i varies from 1 to n in which X_i is the corresponding coded values of a factor, and Y_i is the corresponding response output values (corrosion rate) obtained from the experiment, and n is the total number of combination considered. All the coefficients were obtained applying central composite face centered design using the Design Expert statistical software package. After determining the significant coefficients (at 95% confidence level), the final relationship was developed using only these coefficients. The final empirical relationship obtained by the above procedure to estimate the corrosion rate of friction stir welds of AZ61A magnesium alloy is given below:

$$\text{Corrosion Rate (CR)} = 9.48 - 1.89P - 0.88T + 0.82C + 1.60P^2 + 1.27C^2 \qquad (7)$$

The Eq. 7 is more sensible to analyse the corrosion rate with respect to the corrosion tests parameters. Certain line diagrams were developed with the help of this equation in order to evaluate the sensitivity of the corrosion tests parameters.

3.1. Checking the adequacy of the model

The Analysis of Variance (ANOVA) technique was used to find the significant main and interaction factors. The results of the second order response surface model fitting in the

form of Analysis of Variance (ANOVA) are given in the Table 6. The determination coefficient (r2) indicated the goodness of fit for the model. The Model F-values of (31.30) implies the model is significant. There is only a 0.01% chance that a "Model F-Values" this large could occur due to noise. Values of "Prob > F" less than 0.0500 indicates model terms are significant. In this case P, T, C, P², C² are significant model terms. Values greater than 0.1000 indicate the model terms are not significant. If there are many insignificant model terms (not counting those required to support hierarchy), model reduction may improve the model. The "Lack of Fit F-values" of 1.69 implies the Lack of Fit is not significant relative to the pure error. There is a 28.93% chance that a "Lack of Fit F-values" this large could occur due to noise. Non-significant lack of fit is good. The "Pred R-Squared" of 0.8176 is in reasonable agreement with the "Adj R-Squared" of 0.9349. "Adeq Precision" measures the signal to noise ratio. P ratio greater than 4 is desirable. The ratio of 19.440 indicates an adequate signal. All of this indicated an excellent suitability of the regression model. Each of the observed values compared with the experimental values shown in Table 6 below:

Table 6
ANOVA tests results

| Source	Sum of squares	df	Mean square	F values	p-values	
Model	126.60	9	14.07	31.30	<0.0001	significant
P	49.03	1	49.03	109.11	<0.0001	
T	10.55	1	10.55	23.48	0.0007	
C	9.12	1	9.12	20.29	0.0011	
PT	1.83	1	1.83	4.08	0.0710	
PC	0.047	1	.047	0.10	0.7543	
TC	0.033	1	0.033	0.072	0.7934	
P^2	37.07	1	37.07	82.48	<0.0001	
T^2	3.4E-004	1	3.4E-004	7.6E-004	0.9785	
C^2	23.17	1	23.17	51.55	<0.0001	
Residual	4.49	10	0.45			
Lack of Fit	2.82	5	0.53	1.69	0.2893	not significant
Pure Error	1.67	5	0.33			
Cor Total	131.09	19				
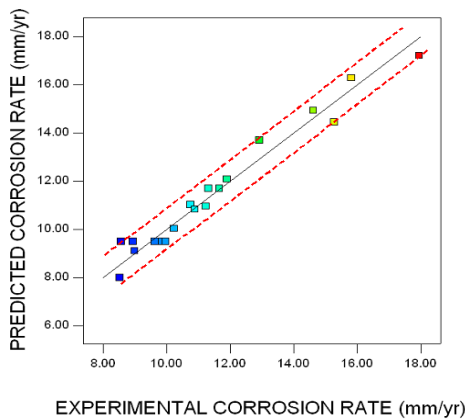
Fig. 5 Correlation graph for response (corrosion rate)

3.2. Validation of the developed models

To validate the developed models, three confirmation experiments were carried out with the process parameters chosen randomly to close the range of experimental parameters. For the actual responses the average of three measured was calculated. Table 7 summarizes the experimental condition, the average actual experimental values, the predicted values and the percentage error. The optimum values of process parameters and the corrosion rate of friction stir welded AZ61A magnesium alloy weldments show the excellent agreement with the predicted values.

Table 7
Validation of tests results

		Experimental details			Results
		Input parameters			Responses
Exp. No.	pH	Exposure Time (hr)	Chloride ion Conc. (M)		Corrosion rate (mm/yr)
21	4	2	0.4	Actual	11.926
				Predicted	11.94
				Error (%)	1.4
22	8	6	0.8	Actual	9.15
				Predicted	9.34
				Error (%)	2.03
23	6	4	0.6	Actual	10.13
				Predicted	10.26
				Error (%)	1.2

4. Results and Discussion

Table 5 shows the corrosion rate obtained from salt fog tests at different pH values, chloride ion concentration and spraying time. Fig. 6 shows the normalized weight loss of salt fog tests samples underwent corrosion. The normalized corrosion rate of salt fog tests samples shown in the bar chart Fig. 7. The highest corrosion rate was observed at pH 3; at neutral pH, the corrosion rate was remained approximately constant and comparatively low corrosion rate was observed in alkaline solution. It was seen that the influence of pH was more at higher concentration as compared to lower concentration in neutral and alkaline solutions [19].
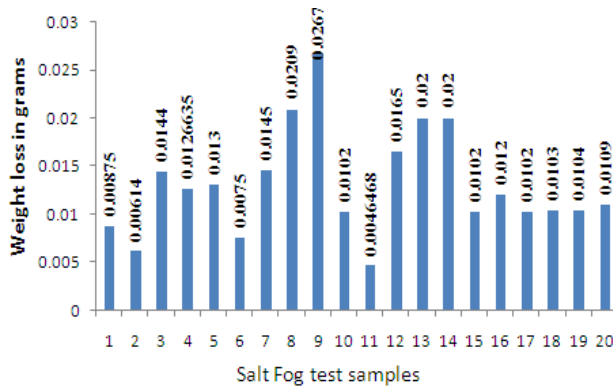

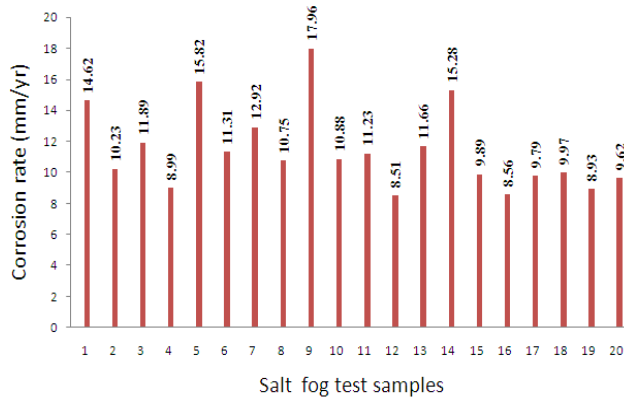**Fig. 6** Normalized weight loss of salt fog tests samples

Fig. 7 Normalized corrosion rate of salt fog tests samples

Also, there exists a correlation between pH, chloride ion concentration and spraying time. The rate of corrosion increases with the increase of chloride ion concentration, and found corrosion resistant with the decrease in chloride ion concentration. At lower pH values, the specimen exhibited a rise in corrosion rate with an increase in chloride ion concentration. But the quantity of this rise was different in such a way that the change in chloride ion concentration at lower concentrations affected the corrosion rate much more as compared to that of higher concentration. It showed that with the increase in chloride ion concentration, the rising rate at corrosion rate decreased that is, the influence of chloride ion concentration was much lower at higher concentrations [19]. Consequently, the rate of corrosion decreased slightly with the increase in spraying time. It resulted from the increase in hydrogen evolution with an increase in spraying time; this is attributed to the corrosion occurring over an increasing fraction of the surface, which is the insoluble corrosion product. The insoluble corrosion product on the surface of the alloy could slow down the corrosion rate [20].

4.1 Effect of chloride ion concentration on corrosion rate

Fig. 8 shows the effect of chloride ion concentration on corrosion morphology and pit morphology of the anodic specimen immersed in NaCl solution of pH 5 for exposure time 5 hrs with different chloride ion concentration of 0.2M, 0.6M and 1M solutions. From the corrosion morphology, the corrosion behavior is consistent with the current understanding that the corrosion behavior of magnesium alloys is governed by a partially protective surface film with the corrosion reaction occurring predominantly at the breaks or imperfections of the partially protective film. However, it was observed that with the increase in chloride ion concentration, the rising rate of corrosion rate decreased. The increase in corrosion rate with increasing chloride ion concentration may be attributed to the participation of chloride ions in the dissolution reaction. Chloride ions were aggressive for magnesium. The adsorption of chloride ions to oxide covered magnesium surface transformed to easily soluble $MgCl_2$ [15]. However, the thermodynamic stability of the magnesium hydroxide is much higher than $MgCl_2$. To dissolve $Mg(OH)_2$, the concentration of chlorides must be higher than hydroxide ions. It was also observed that decreasing of pH decreases the stability of the hydroxide was evident from the Fig. 8. It shows that the corrosion rate was altered much in the lower pH and higher chloride ion concentrations. The welds exhibited a rise in corrosion rate with the increase in Cl⁻ concentration and thus the change of Cl⁻ concentration affected the corrosion rate much more in higher concentration solutions than in lower concentration solutions.
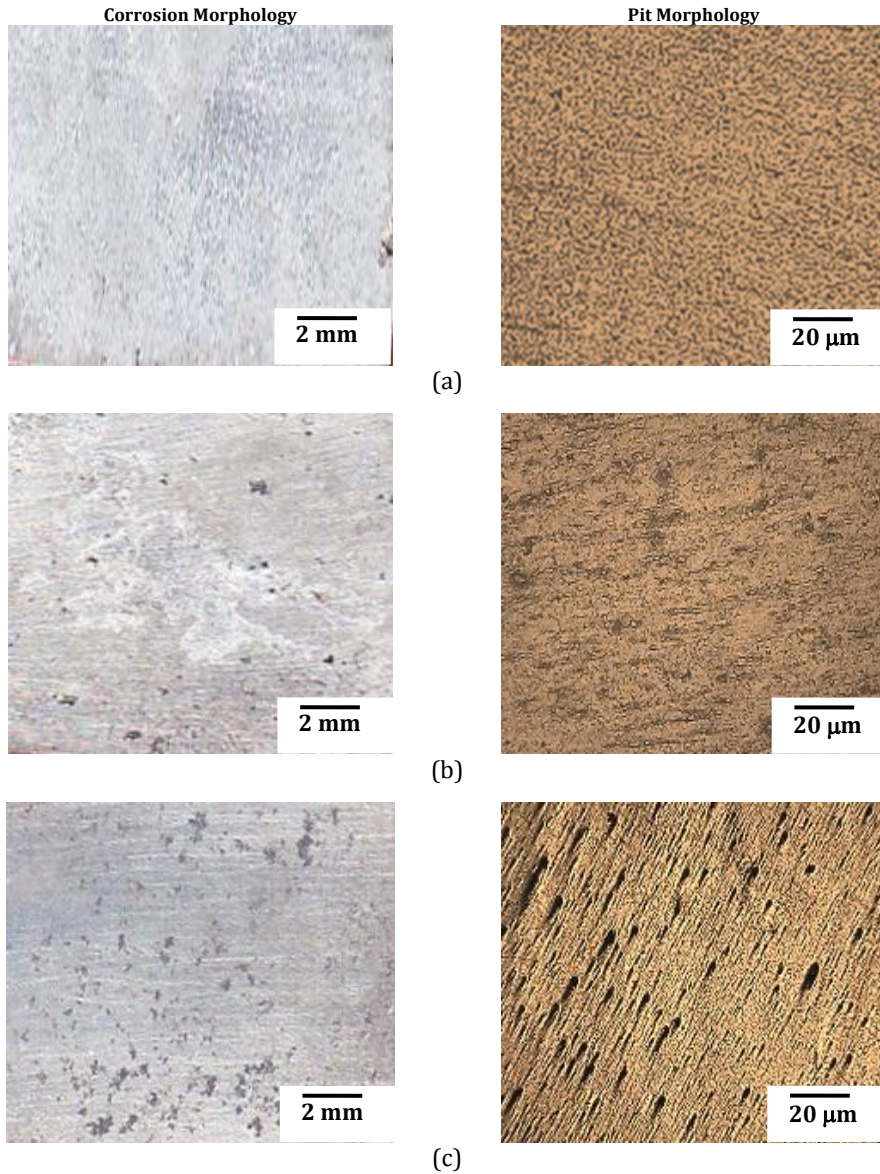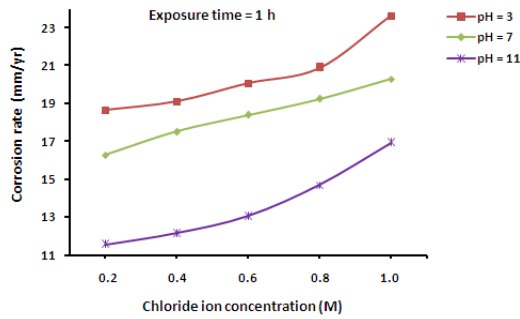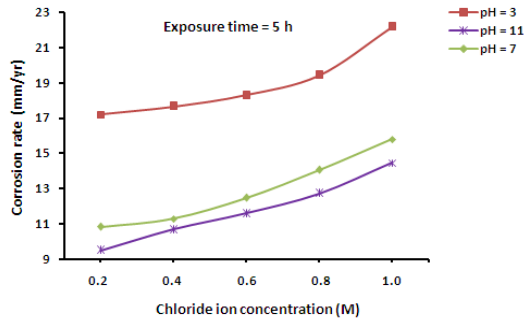
Corrosion Morphology   **Pit Morphology**

(a)

(b)

(c)

Fig. 8 Effect of (a) 0.2M, (b) 0.6M, (c) 1M chloride ion concentration on corrosion morphology and pit morphology

From the microstructure of FSW joints after salt fog tests at different pH values, chloride ion concentration and spraying time, it showed that the alloy exhibited a rise in corrosion rate with the increase in Cl⁻ concentration. When the concentration of Cl⁻ in NaCl solution was higher, promoted the corrosion, the corrosive intermediate (Cl⁻) would be rapidly transferred through the outer layer, and reached the substrate of the alloy surface [20]. Hence, the corrosion rate was increased. This corrosion behavior is consistent with the current understanding that the corrosion behavior of magnesium alloys is governed by a partially protective surface film with the corrosion reaction occurring predominantly at the breaks or imperfections of the partially protective film [21].

157

Fig. 9 shows the graph developed from the Eq. 7 to represent the effect of chloride ion concentration on corrosion rate. The graph shows clearly that the resistivity of corrosion was low with the increase in chloride ion concentration. From the morphological studies, it was observed that, at lower concentration, the surface of the specimen relatively slightly corroded; while severely corrode in the higher concentrations. Moreover, the welds exhibited a rise in corrosion rate with the increase in Cl⁻ concentration, and thus the change of Cl⁻ concentration affected the corrosion rate much more in higher concentration solutions than that in lower concentration solutions.

(a)

(b)
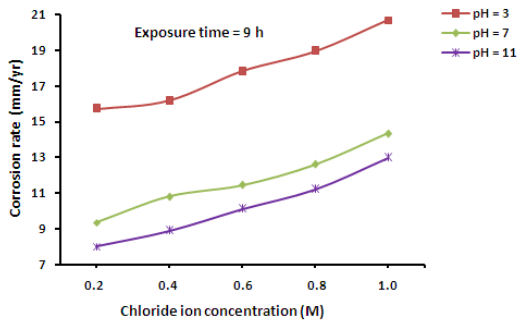
(c)

Fig.9 Effect of chloride ion concentration on corrosion rate (a) 1h, (b) 5h and (c) 9h exposure time

4.2 Effect of spraying time on corrosion rate

Fig. 10 shows the effect of chloride ion concentration on corrosion morphology and pit morphology of the specimen sprayed in NaCl solution of pH 5 for exposure time 5 hrs with different chloride ion concentration of 0.2M, 0.6M and 1M solutions. From the corrosion morphology, with the increase in immersion time, the corrosion rate decreases. The increase in immersion time enhanced the tendency to form the corrosion products, which accumulated over the surface of the samples. It results that there was an increase in hydrogen evolution with the increasing immersion time, which tends to increase the concentration of OH^- ions strengthening the surface from corrosion causing further. This is attributed to corrosion occurring over increasing fraction of the surface was observed, which is the insoluble corrosion products [22]. The insoluble corrosion products on the surface of the alloy could slow down the corrosion rate.

During the experiment, some black areas appeared initially, these areas become larger and additional similar areas appear with the increase in time. It was characterized by the observation of localized attack and many upheavals with pitting occurrence. From the pit morphology, it was observed that the grain is refined, and quite a lot of β particles were distributed continually along the grain boundary. In this case, β phase particles cannot be easily destroyed and, with the increase of corrosion time, the quantity of β phases in the exposed surface would increase and finally play the role of corrosion barrier. Although, there are some grains of α phase still being corroded, most of the remaining α phase grains are protected under the β phase barrier, so the corrosion resistance improved with the increase of spraying time [22].

Fig. 11 shows the graph represents the effect of spraying time on corrosion rate. The graph shows clearly that the corrosion rate was decreased with the increase in spraying time. It results that there was an increase in hydrogen evolution with the increasing spraying time, which tends to increase the concentration of OH^- ions strengthening the surface from corrosion causing further. In addition, it turns the surface of the specimen from activity to passivity. Thus, the rate of corrosion decreases with the increase in spraying time.

4.3 Effect of pH values on corrosion rate

Fig. 12 shows the effect of pH on corrosion morphology and pit morphology of the corrosion tests specimen sprayed in 0.6M concentration of NaCl for 5 hrs with different pH values of pH 3, pH 7 and pH 11. From the corrosion morphology, the surface of the specimen sprayed to low pH solution constituted more corrosion products, thus corrosion occurred severely. As denoted earlier, at every chloride ion concentration and immersion time, the welds usually exhibited a decrease in corrosion rate with increase in pH. In neutral pH, the corrosion rate remained constant, and comparatively low corrosion rate was observed in alkaline solution. It was seen that the influence of pH was more at higher concentration as compared to lower concentration in neutral and alkaline solutions [19].
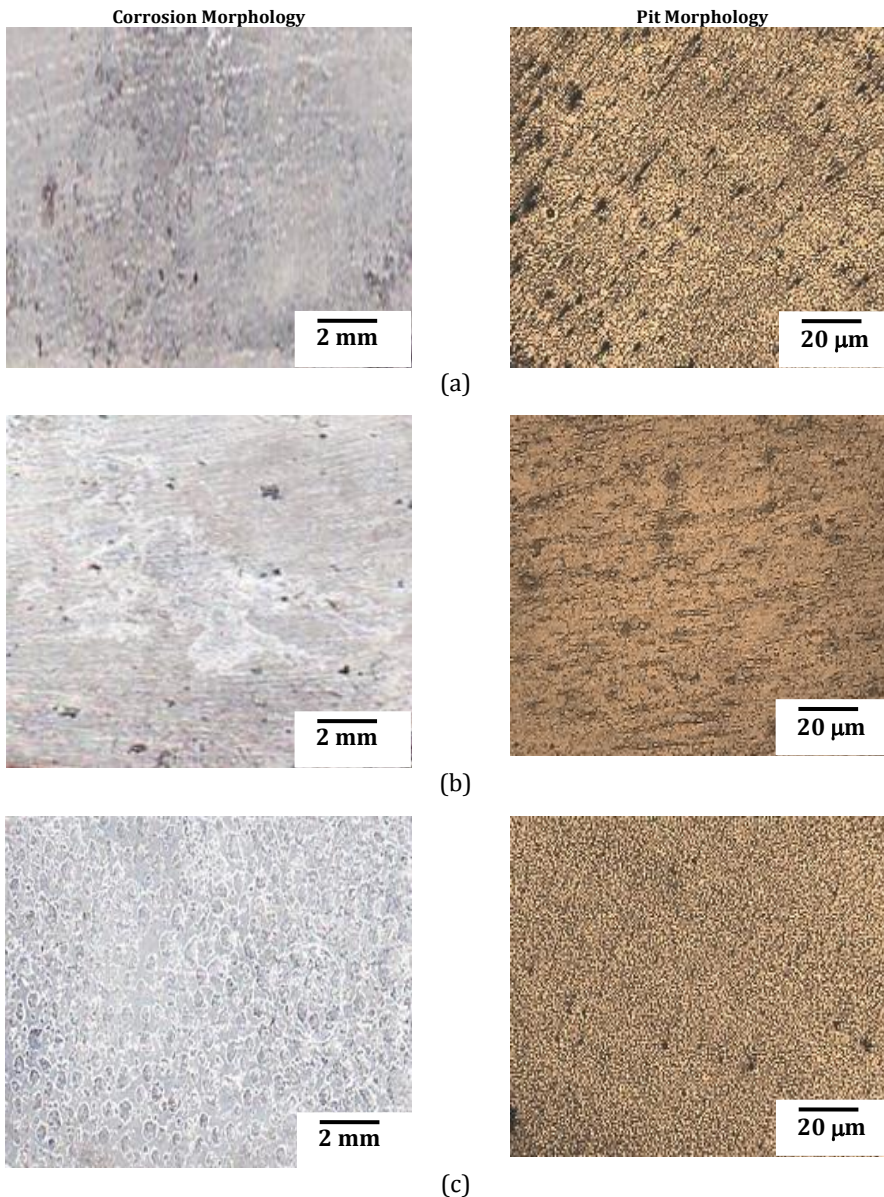
Corrosion Morphology   **Pit Morphology**

(a)

(b)

(c)

Fig. 10 Effect of (a) 1h, (b) 5h and (c) 9h spraying time on corrosion morphology and pit morphology

From the pit morphology, it was observed that the matrix shows the pitting marks and the pitting corrosion that has taken place at the friction stir welded microstructure. The particles are Mn-Al compound and fragmented $Mg_{17}Al_{12}$. The numbers of pits were more in the joints when sprayed with the solution of low pH. Hence, the corrosion rate increases with the decrease in pH values. Since the increase of grain and grain boundary in the joints, the grain boundary acts cathodic to grain causing micro galvanic effect. The presence of micro-galvanic effect between the α-phase and the β-phase, formed due to the presence of aluminum. The β-phase generally acts an effective cathode which

accelerates the corrosion of the adjacent α-phase [20]. Hence, the high corrosion rate occurs at a certain ratio of anodic to cathodic area.
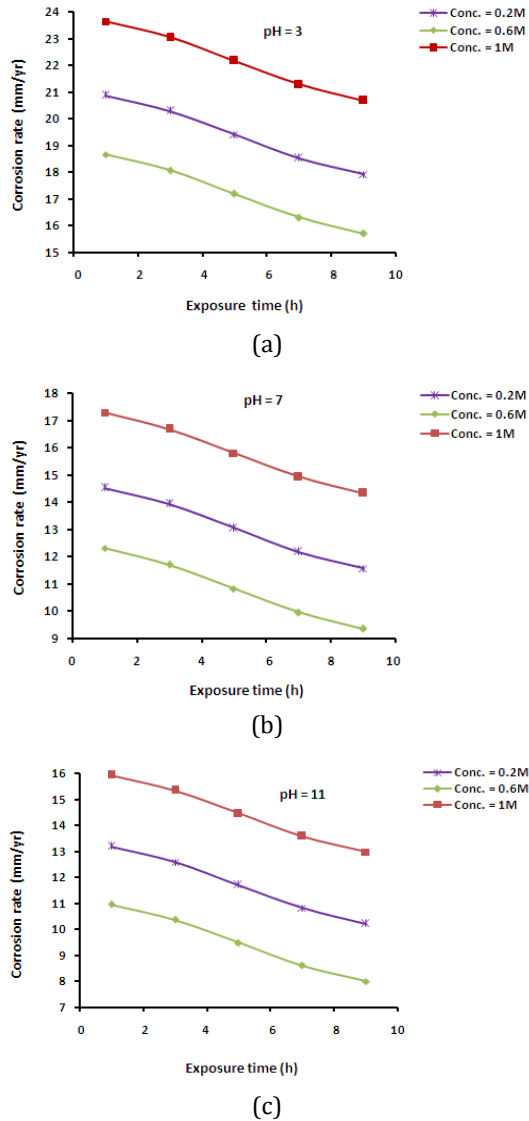

(a)

(b)

(c)

Fig.11 Effect of spraying time on corrosion rate (a) pH 3, (b) pH 7 and (c) pH 11

As it can be expected for active metals, the rate of corrosion of these metallic materials in acidic medium is relatively high compared to that in neutral or basic solutions. This can be explained by the formation of a barrier layer of $Mg(OH)_2$, which is insoluble; in basic solution[21]. In acidic solutions, the barrier layer is completely soluble, and hence relatively high corrosion rates were recorded. In neutral solutions, the barrier magnesium hydroxide layer is partially soluble and so a decrease in the corrosion rate was recorded. Corrosion tends to be concentrated in the area adjacent to the grain boundary until eventually the grain may be undercut and fall out [22]. It means that the pH values were one of the major factors of corrosion rate.
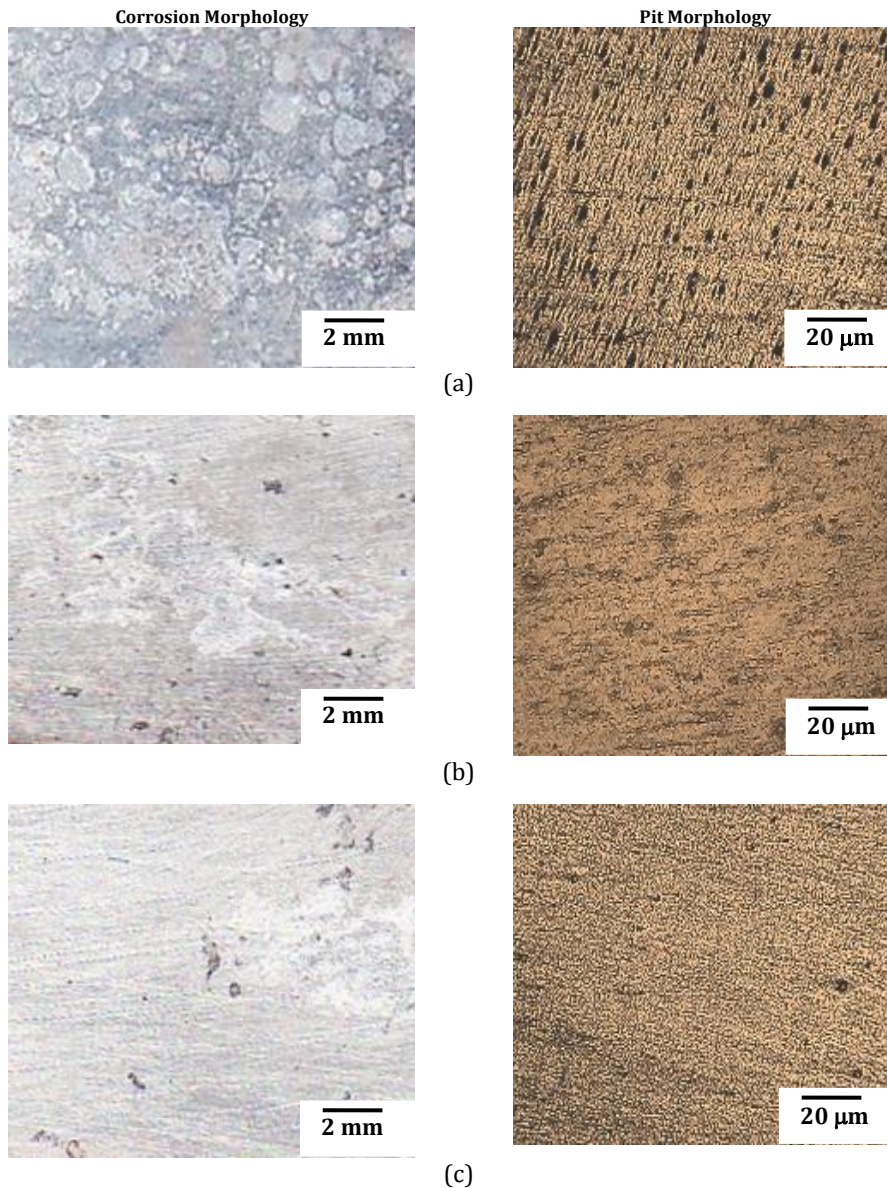
Corrosion Morphology   **Pit Morphology**

(a)

(b)

(c)

Fig. 12 Effect of pH on corrosion morphology and pit morphology (a) pH 3, (b) pH 7and (c) pH 11

Fig. 13 shows the graph representing the effect of pH on corrosion rate. The graph shows clearly that the corrosion rate was decreased with the increase in pH values. At every chloride ion concentration and immersion time, the FS welds usually exhibited a decrease in corrosion rate with an increase in pH. In neutral pH, the corrosion rate remained constant, and comparatively low corrosion rate was observed in alkaline solution. It was seen that the influence of pH was more at higher concentration as compared to lower concentration in neutral and alkaline solutions.
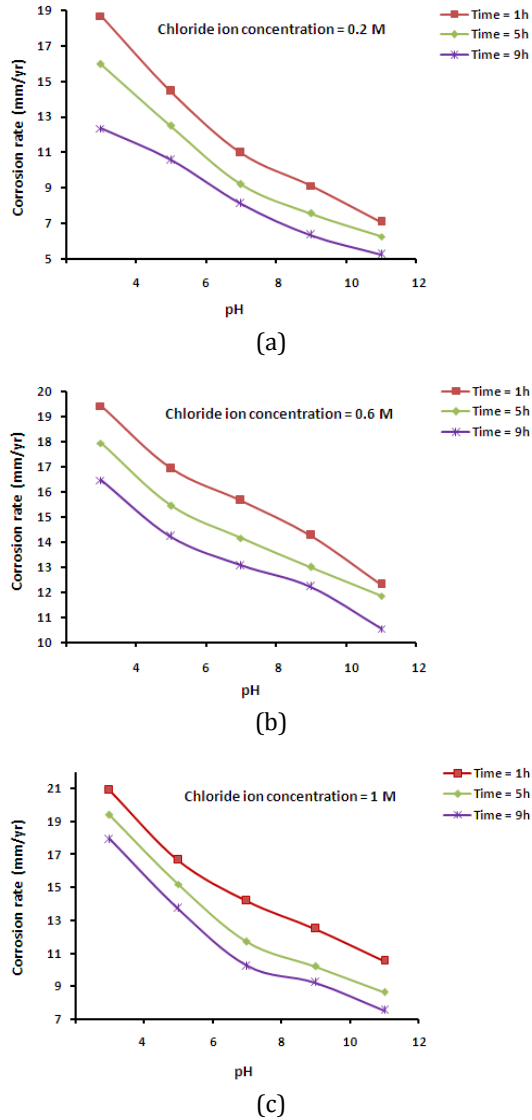
Fig. 13 Effect of pH on corrosion rate (a) 0.2M, (b) 0.6M and (c) 1M chloride ion concentration

4.4 Microstructural Characterization

Fig. 14 shows the surface texture of the specimens underwent salt spray corrosion sprayed for (a) 2.62, (b) 5, and (c) 7.38 hrs observed under SEM. Fig. 14a shows the specimen comprised of more localized attack. With pH as a factor, the less pH value tends to attack very localized on the surface, and later, it penetrates to the substrates, causing higher corrosion and its rate. The localized attack in the specimen formed at the grains. Since the increase in grain and grain boundary in the FSW welds, the grain boundary acts cathodic to grain, enhancing micro-galvanic effect. Corrosion tends to be concentrated in the area adjacent to the grain boundary until eventually the grain may be undercut and fall out [20]. The protective layer formed at pH 9.38 is stable and non-degradable. At

163

higher pH values, the eutectic α-phase and the β-phase were completely protected under the hydroxide layer.

Fig. 14b shows the specimen comprised of the corrosion products remains spongy and non-adherent. When more Cl- in NaCl solution promoted the corrosion, the corrosive intermediate (Cl-) would be rapidly transferred through the outer layer and reached the substrate of the alloy surface [23]. The exposed surfaces during fog tests were continuously exposed to dissolved chloride ions, meaning new pits could form at any point. The corrosion behavior of the FSW AZ61A magnesium alloy welds is governed by the partially protective surface film. However, with a chloride ion concentration of 0.36M, the Gibb's free energy to form the metal chloride layer is -591.8 kJ/mol. But the free energy of the initial protective layer MgO is -596.3 kJ/mol. When the chloride ion concentration is 0.84M, the Gibb's free energy formed is higher, compared to the free energy of the protective film. The surface of the specimen shows more cracks over the corrosion products, where the Cl- penetrates into the surface. More Cl- in the NaCl solution promotes corrosion.

From Fig. 14c, it was observed that lamellar fine structures which causing a resistivity towards corrosion. The lamellar structures were found to be the β-phase. The β phase particles cannot be easily destroyed and, with the increase of corrosion time, the quantity of β phases in the exposed surface would increase and finally play the role of corrosion barrier. Thus, there proved that, with an the increase in the spraying time, there exists a resistivity towards corrosion. With the increase of exposure time, the local pH of the electrolyte increases fairly as the Mg alloy corrodes, with the precipitation of $Mg(OH)_2$, a protective layer. Thus, the alkalization should be propitious to the formation of a passive film, which can protect the alloy. The insoluble corrosion products formed on the surface of the alloy could slow down the corrosion rate.
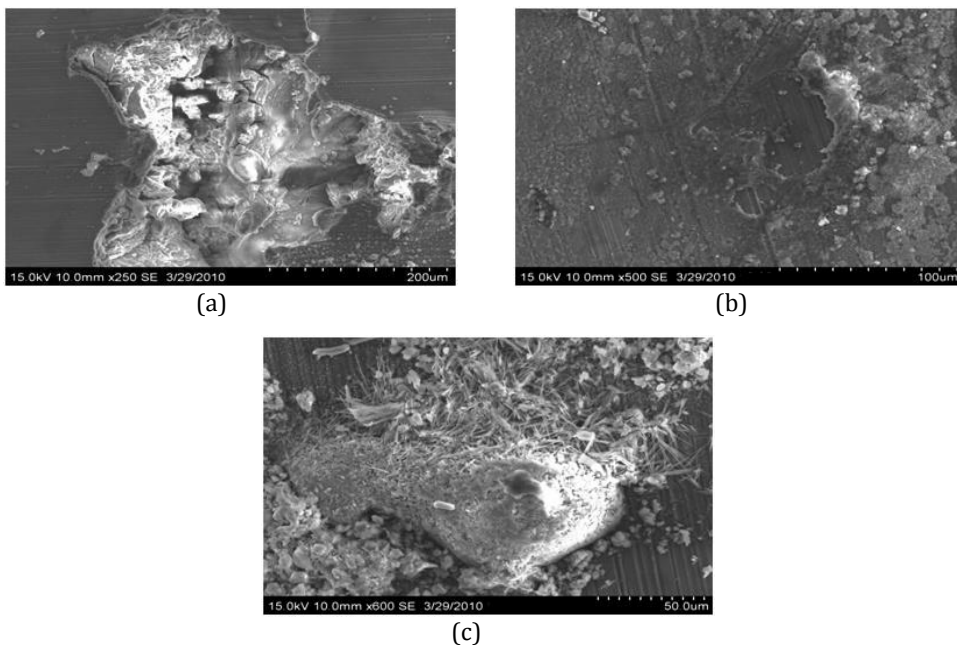

(a)   (b)

(c)

Fig. 14 SEM graph of salt fog corrosion tests (a) pH 4.62, Cl- 0.36M, 2.62 hrs, (b) pH 7, Cl- 0.60M, 5 hrs and (c) pH 9.38, Cl- 0.84M, 7.38 hrs

Fig. 15 shows the XRD result of the corrosion products. All the characteristic peaks originate from the metallic Mg substrate and the β Phase. $Mg(OH)_2$ is the dominant product in the corrosion zone. $Mg(OH)_2$ (brucite) has a hexagonal crystal structure, and undergoes easily basal cleavage causing cracking and curling in the film [24]. Furthermore, it also comprises of several β Phase of small peaks namely, $Mg_{17}Al_{12}$.
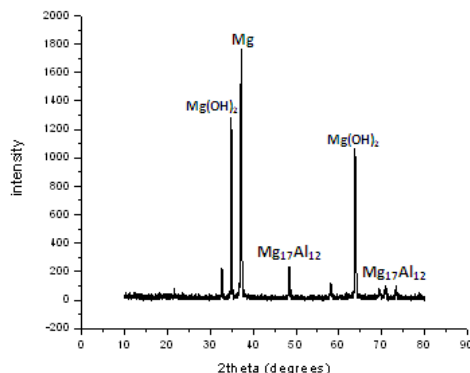

Fig. 15 XRD pattern of salt fog corrosion tests specimen

5. Conclusions

From the results in this study, the following conclusions can be written:

- Chloride ions were aggressive on magnesium alloy. The adsorption of chloride ions to oxide covered magnesium surface transformed to easily soluble $MgCl_2$. Thus, corrosion developed more seriously with the increase of chloride ion concentration.
- The corrosion is rate closely related to the spraying time. The initial corrosion products provided protection for metal substrate and delayed further attack. Thus, the corrosion rate decrease with the increase of spraying time.
- The pH of the solution was one of the major factors for the corrosion resistance of AZ61A magnesium alloy welds. As with the increase on pH, the corrosion rate was decreased; as a result, the corrosion resistance was improved.

Acknowledgements

References

1. Zeng RC, Dietzel W, Zettler R and Chen J. Microstructure evolution and tensile properties of friction-stir-welded AM50 magnesium alloy. Transaction of Nonferrous Metal Society of China, 2008; 18: 76 – 80.
2. Zeng RC, Dietzel W, Huang WJ, Kainer KU, Zettler R and Zhang J. Review of studies on corrosion of magnesium alloys. Transaction of Nonferrous Metal Society of China, 2006; 16: 763 – 771.

3. Nagasawa T, Otsuka M, Yokota T and Ueki T. Structure and mechanical properties of friction stir weld joints of magnesium alloy AZ31. Magnesium Technology, 2000; TMS: 383 – 387.
4. LeBozec N, Jönsson M and Thierry D. Atmospheric corrosion of magnesium alloys: Influence of temperature, relative humidity, and chloride deposition. Corrosion, 2004; 60: 356 – 362.
5. Zhao MC, Liu M, Song G and Atrens A. Influence of pH and chloride ion concentration on the corrosion of Mg alloy ZE41. Corrosion Science, 2008; 50(11): 3168 – 3178.
6. Hawke DL, Hillis JE, Pekguleryuz M and Nkatusugawa I, in: Avedesian MM, Baker H(Eds.). Magnesium and Magnesium Alloys. ASM International, Materials Park, 1999: 194 – 210.
7. Abady MG, Hillal HN, El- Rabieee M and Badary AN. Effect of Al content on the corrosion behavior of Mg-Al alloys in aqueous solutions of different pH. Electrochemical Acta, 2010, 55: 6651 – 6658.
8. Merins MC, Paradr A, Arrabal R and Morine S. Influence of chloride ion concentration and temperature on the corrosion of Mg-Al alloy in salt fog. Corrosion science, 2010, 52: 1696 – 1764.
9. Song G, Atrens A, Wu X and Zhang B. Corrosion behavior of AZ21, AZ501, AZ91 in NaCl. Corrosion Science, 1998; 40: 1769 – 1791.
10. Ambat R, Aung NN and Zhao W. Evaluation of microstructural effects of corrosion behavior of AZ91 D Mg alloy. Corrosion Science, 2000; 42: 1433 – 1455.
11. Hara N, Kobayashi Y, Kagaya D and Akao N. Formation and breakdown of surface films on magnesium and its alloys in aqueous solutions. Corrosion Science, 2007; 49: 166 – 175.
12. Schumtz P, Guiaumin V, Lilard RS, Lilard JA and Frankela GS. Influence of dichromate ions on corrosion process on pure magnesium. Journal of electrochemical society, 2003; 150: B99 – B110.
13. Zeng RC, Chen J, Dietzel W, Zettler R, F. Dos Santos J, Nascimento ML and Kainer KU. Corrosion of friction stir welded magnesium alloy AM50. Corrosion Science, 2009; 51: 1738 – 1746.
14. Song G and Atrens A. Understanding magnesium corrosion – a framework for improved alloy performance. Advanced Engineering Materials. 2003; 5: 837 – 858.
15. Altun H and Sen S. Studies on the influence of chloride ion concentration and pH on the corrosion behavior of AZ63 magnesium alloy. Materials & Design, 2004; 25: 637 – 643.
16. Song Y, Shan D, Chen R and Han EH. Effect of second phases on the corrosion behavior of wrought Mg-Zn-Y-Zr alloy. Corrosion Science, 2010: 52: 1830 – 1837.
17. Dhanapal A, Boopathy SR and Balasubramanian V. Developing an empirical relationship to predict the corrosion rate of friction stir welded AZ61A magnesium alloy under salt fog environments. International Journal of Materials and Design, 2011; 32: 5066 – 5072.
18. Dhanapal A, Boopathy SR and Balasubramanian V. Influence of pH values, chloride ion concentration and immersion time on corrosion rate of friction stir welded AZ61A magnesium alloy weldments. International Journal of Alloys and compounds, 2012: 523: 49 – 60.
19. Neil WC, Forsyth M, Howlettt PC, Hutchison CR and Hinton BRW. Corrosion of magnesium alloy ZE41 – The role of microstructural features. Corrosion Science, 2009; 51: 387 – 394.

20. Lafront AM, Zhang W, Jin S, Tremblay R, Dube D and Ghali E. Pitting Corrosion of AZ91D and AJ62x magnesium alloys in alkaline chloride medium using electrochemical techniques. Electrochimica Acta, 2005; 51: 489 – 501.
21. Zhao MC, Liu M, Song GL and Atrens A. Influence of pH and chloride ion concentration on the corrosion of Mg alloy ZE41. Corrosion Science, 2008; 50: 3168 – 3178.
22. Gao L, Zhang C, Zhang M, Huang X and Sheng N. The corrosion of a novel Mg-11Li-3Al-0.5RE alloy in alkaline NaCl solution. Journal of alloy compounds, 2007: 285 – 289.
23. Xin R, Li B, Li L and Liu Q. Influence of texture on corrosion rate of AZ31 Mg alloy in 3.5wt% NaCl. Materials and Design, 2011: 4548 – 4552.
24. Balasubraminan P, Zetler R, Blawert C and Dietzel W. A study on the effect of plasma electrolytic oxidation on the stress corrosion cracking behavior of wrought AZ61 Mg alloy and its friction stir welding. Material and characteristics, 2009, 60: 289 – 389.